Supplementary Information

Hoebe et al. 2024. Early Holocene inundation of Doggerland and its impact on hunter-gatherers: an inundation model and dates-as-data approach. *Quaternary International*

1. Inundation model workflow
2. paleoDEM construction (Freek Busschers)
3. SLS construction
4. Radiocarbon workflow and dataset description
5. Inundation model output

1 Inundation model workflow

In the workflow described below we used open source software QGIS (v3.22) with the python console and R (v4.2.1) for data preparation, analysis and plotting.

1.1 DEM raster layers

Use a digital elevation model as a basis for modelling. As a modern DEM/Bathymetric model we used GEBCO at a 5x5 km resolution. A paleoDEM was constructed by F.S. Busschers (this paper, see SI-2: paleoDEM construction). This paleoDEM raster was substracted from the GEBCO DEM/Bathy using the raster calculator in QGIS (BATHY.tif - paleoDEM.tif = Holocene.tif sedimentation, Figure 3b).

1.2 Inundation Model output

Given a DEM, any sea level curve can be used to simply inundate this DEM with the raster calculator. Either a timestep specific DEM can be generated by extracting the ESL or RSL value(s) of the specific timestep from the DEM, or raster layer can be generated with categories based on defined conditions.

1.2.1 IM000/IM100 Bathy/pDEM x ESL

We used an ESL curve provided by Lambeck 2014, corrected for the North Sea region (multiplied by 0.85). Create a vector by sampling the curve at 250y intervals, saved as a csv, which can then be used in inundation modelling by subtracting those values from the DEM. This output can be generated manually with the raster calculator for a specific timestep, or automated with the python console (see ‘IM000-IM100.py’).

1.2.2 IM010/IM110 Bathy/pDEM x SLS

For GIA based model output, sea level surfaces (SLS) need to be constructed (see SI-3 and ‘SLS.R’).

a) Make sure the GIA model output locations have an acceptable spatial coverage for the chosen spatial interpolation method. We selected GIA curves provided by Vink et al. 2007, Kuchar et al. 2012 and Shennan et al. 2018 and extracted the RSL values at 250y intervals. The curves from the different sources were compared and corrected based on SLIPs (see section 3.1.2, SI-3). Curves that do not cover the entire timeframe were extrapolated backwards based on the progression of other curves that had better coverage (see SI-3 and ‘SLS.R’ for workflow). Create points for the GIA curves in QGIS and save as shapefile. Generate raster layers for each timestep by interpolating (see ‘SLS.py’). We used SAGA's Thin Plate Spline, which is suitable to interpolate data with irregularly spaced points and for creating smooth surfaces with flexible bending characteristics. We used a regularisation parameter of 0.0001.

b) The generated spatial interpolation provides continuous relative sea level values per timestep as a raster file, which can be subtracted from a DEM with the raster calculator. This output can be generated manually for a specific timestep, or automated with the python console (see ‘IM010-IM110.py’).

1.2.3 IM011/IM111 & IM012/IM112 Bathy/pDEM x SLS + corrections

Finally we can correct these inundation models for basin background subsidence (IM011/IM111) and coastal peat growth (IM012/IM112).

a) A BBS raster was used with the rate of background subsidence in meters per ka (provided by TNO). The values were divided by 4 using the raster calculator to get values per 250y timestep. A BBS multiplier csv was made with a timestep column (calBP) and the corresponding multiplier. That is: the number of 250y timesteps passed between the relevant timestep and the present. For example, for 12000 calBP this is a multiplier of 48, and 7000 calBP this is a multiplier of 28. In the research area maximum BBS in m/ka is ca. -0.24, which is a rate of -0.06 per 250y timestep. This negative value has to be substracted from (i.e. the absolute value has to be added to) a DEM of the current situation to correct for the downward land motion since that particular timeframe. This means a maximum BBS correction of +1.68m at 7000 calBP and +2.88 at 12000 calBP.

b) Peat growth took place prior to inundation during the Early Holocene. Where these peat layers have been documented below sediments related to inundation/marine transgression, their pre-compaction thickness is estimated at ca. 0.5m at 10000 calBP and 1 meter at 8000 calBP. Assuming a constant growth rate and onset of peat growth at 11500 calBP, a peat correction .csv was made with a correction value per timestep. This correction value is added to the DEM when determining the sea-land boundary (note that it is not appropriate to add this value to the DEM as a whole as this concerns a correction for elevation change in coastal areas only). To visualise the effect of this correction, timestep specific DEMs were made by substracting the 10 and 9ka SLS from the pDEM and visualising the relevant correction values below relative sea level (Figure 6b).

c) These corrections are added to the raster calculator expression (see ‘IM011-IM111_IM012-IM112.py’).

For all abovementioned inundation models, simple coastline models can be generated by changing the raster calculator expression to

```
((DEMresult+c)<= sealevel) \*1 + ((DEMresult+c)>sealevel) \*2.
```

The output of coastline layers can be combined into one layer by adding them all together in raster calculator (Figure 11: Coastline dating). By vectorising the result and calculating the area of each timestep inundation polygon, we arrive at the inundation by timestep output (Figure 12: Inundation area).

1.3 Cumulative correction effect

The correction effect of all inundation model improvements was calculated for 10ka (as an example) with raster calculator (except coastal peat correction). The correction effect rasters show what effect each model component has on the basic Bathy x ESL model. Holocene sediment thickness was converted to negative values, showing what is subtracted from the bathymetry to arrive at paleoDEM. ESL at 10ka was added to the GIA at 10ka to show the spatially differential effect of glacio-isostatic adjustment, resulting in a correction effect map in meters above and below ESL. Finally BBS was converted to positive values, and multiplied to provide the number of meters subsided since 10ka. These three correction effects (Figure 7a-c) together form the spatially differential culmulative correction effect (Figure 7d). This visualises the difference between IM112 and IM000.

1.4 Calculating inundation rate

Inundation rate per timestep can be calculated by performing a raster cell count. This is done by processing a raster layer unique values report and combining the results of each inundation model timestep layer into one csv file (see ‘inundation rate data.py’). From the resulting data we calculate the difference in the area of water between a given timestep and the preceding timestep, which can be plotted as a histogram (see ‘inundation rate.R’).

1.5 Other output

The distribution of sediment coverage on submerged coastal areas (Figure 16) was calculated by taking the Holocene sediment raster and defining sediment thickness classes (0-0.5, 0.5-5, 5-10, 10-25m). These were saved as raster mask layers, which were then used to extract the dates of submerged coastal zones (Figure 11) that these Holocene sediments cover. A raster cell count for each result gives the area in km2 for each sediment cover class. This was then visualised in a histogram to show the age of coastal zones in the research area that are covered by significant Holocene sediments. This is an indicator of potentially favourable preservation conditions of coastal contexts of specific age, but also of low accessibility.

Raster cell counts were also used to calculate the changing relative proportions of landscape zones in the research area using IM112 output. The proportion of total area of inland, lowland, wetland and sea changed over time. The plot (Figure 17) illustrates that given the inundation history in the research areas this landscape change alone would lead to changing proportions and overall densities in a dates-as-data approach.

2 PaleoDEM construction

FS Busschers

In this study we constructed a new composite grid of the top of the Pleistocene (m -MSL) for the southern North Sea, incorporating data from the onshore and offshore regions of the Netherlands, Lower Saxony and Belgium. Table 2.1 lists the resources used to combine in the paleoDEM assembled for this study.

	Source	Coverage	Resolution
Bathymetry and DEM			
	General Bathymetric Chart of the Oceans GEBCO (download.gebco.net)	Worldwide	1m, 250×250m
paleoDEM			
1	Geopotenzial Deutsche Nordsee GPDN (www.geopotenzial-nordsee.de)	Niedersachsen offshore	2m, isopach
2	Niedersächsischen Bodeninformationssystems NIBIS (nibis.lbeg.de)	Niedersachsen onshore	2m, isopach
3	Offshore mapping programme TNO (FSB this paper)	Netherlands offshore	1cm, 100×100m
4	Rijksdienst voor het Cultureel Erfgoed RCE (www.cultureelerfgoed.nl)	Netherlands onshore	1cm, 100×100m
5	Drowned Landscapes of the Belgian continental Shelf (De Clercq 2018)	Belgium offshore	1cm, 100×100m
6	Databank Ondergrond Vlaanderen DOV (dov.vlaanderen.de)	Belgium onshore	1cm, 100×100m

SI Table 2.1: Source, coverage, and resolution (x, y) of the different DEMs used in inundation modelling.

For the Dutch onshore and offshore zones, we used all available stratigraphic codes (v2003) that were available in the DINO database managed by TNO-GDN (www.dinoloket.nl; accesses 01-01-2023). We used data points that indicate the top of the Pleistocene surface and which show no signs of major posterior erosion by younger channels. The total dataset included 242,128 borehole data points of which 1694 points were located in the offshore area, the latter including 392 points where the Basal Peat Bed was identified using a Python script. This dataset was complemented with borehole information from two profiles (Hijma et al. 2012; profiles VIII & IX) and contour lines showing the position of the Silver Pit (Westerhoff et al., 2003).

For the Belgium onshore zone, we used the grid of the base of the Calais and Dunkerque Members of the Geological 3D model of Flanders G3Dv3 managed by Databank Ondergrond Vlaanderen (DOV; dov.vlaanderen.be; accessed 01-02-2023). All data was transferred into MSL and grid values below -15m MSL were removed, assuming these represented areas of major younger erosion. For the offshore Belgium zone, we used the grids of De Clercq (2018; De Clercq et al. 2016) showing the top of the Pleistocene and top of the Paleogene. Values from the top Pleistocene grid were complemented with data from the top Paleogene grid in cases where the first grid had no-data. From the resulting grid we only selected the grid values higher than -33m MSL in order to make the best approximation of the top Pleistocene paleo surface before major Holocene erosion occurred.

For the German onshore part (Lower Saxony) we used the grid relief of the Holocene basis from the LBEG NIBIS Kartenserver (nibis.lbeg.de; accessed 01-01-2023). From this grid we only selected the grid values higher than -18m MSL in order to make the best approximation of the top Pleistocene paleo surface before major Holocene erosion occurred. For the German offshore zone we used the grid showing the depth of the Holocene base 2m contour from the GPDN Nordsee Kartenserver (geopotenzial-nordsee.de; v26-11-2013). In cases where the German offshore and onshore grids overlapped, data from the latter grid were removed.

All grids were transformed into point data using one point per grid cell. The point and contour line data were reprojected to UTM 31N (EPSG:32631), with zones of overlap removed. This ensemble of top Pleistocene depths was then interpolated using 2*2km grid cells, using a spline algorithm (ESRI Arcmap v10.6).

3 SLS construction

3.1 GIA model details

Glacio-isostatic adjustment curves from Shennan et al. (2018), Kuchar et al. (2012) and Vink et al. (2007) were used as a basis of the sea level layers. Vink et al. (2007) reviewed 238 SLIPs for the eastern part of the southern North Sea (*ibid*: 3252-58) and provide best-fit smooth RSL curves for the last 10ka, from 24 locations between Flanders, Schleswig-Holstein and the Dogger Bank (*ibid*: 3267-69). These are based on a spherically symmetric, compressible, Maxwell-viscoelastic Earth model (PREM; Dziewonski & Anderson 1981; see Vink et al. 2007: 3259-60, Steffen & Kaufman 2005) and the global ice model RSES (Research School of Earth Sciences Canberra; Vink et al. 2007: 3260). RSL curve error limits are dependent on the best-fit earth model's standard deviation, ranging from 0.5 – 1 meter depending on the sub-region. The sub-regions and their earth model parameters are 1) Belgium: lithosphere thickness H_{1}=140 km, upper mantle viscosity $\eta_{UM}=2\times10^{21}$ Pa s, and a lower mantle viscosity $\eta_{LM}=2\times10^{22}$ Pa s; 2) the Netherlands: H_{1}=100 km, $\eta_{UM}=7\times10^{20}$ Pa s, $\eta_{LM}=7\times10^{21}$ Pa s; and 3) Germany: H_{1}=80 km, $\eta_{UM}=7\times10^{20}$ Pa s, $\eta_{LM}=7\times10^{21}$ Pa s. The German coastal locations during the Early Holocene have this higher uncertainty of ca 1 meter (Vink et al. 2007: 3267).

Shennan et al. (2018) present over 1500 SLIPs for Britain and Ireland across 86 regions, and review Bradley's GIA models BRADLEY2011 and BRADLEY2017 which have 21 locations relevant to southern North Sea inundation, from southern Scotland to Sussex, to the Dogger Bank (Bradley et al. 2011; Bradley 2011; Shennan et al. 2018: 146-47). The GIA models are based on a best-fit earth model for the British Isles with parameters H_{1}=71 km, $\eta_{UM}=5\times10^{20}$ Pa s, $\eta_{LM}=3\times10^{22}$ Pa s with the same basic construction as the earth models used in Vink (Bradley et al. 2011: 544-45), an ice sheet model for the BIIS (Brooks et al. 2008), and a model of Late Pleistocene ice history, and ocean mass redistribution calculations based on an ESL model (Bradley et al. 2011: 544; Kendall et al. 2005; Mitrovica & Milne 2003; Farrel & Clark 1976).

3.2 RSL curve modifications

Because models were optimised for their specific regions (British Isles and the southeastern North Sea respectively), they correspond poorly in the centre of the research area, around the Doggerbank. First all curves were interpolated at 50 year timesteps using linear approximation (approx() function in R). Sea level indication points were then used to check, and if necessary, correct GIA model curves in this central Northsea area.

The location of GIA model output curves from Kuchar (0), Vink (1-24) and Shennan (122-165, corresponding to 22-65 in Shennan et al. 2018) is given in Figure 1a, with locations of sea level indication points (SLIPs) and upper limiting points (ULPs) close to the model output locations (corresponding id numbers with decimals). The curves and points themselves are given in Figure 1a and b.

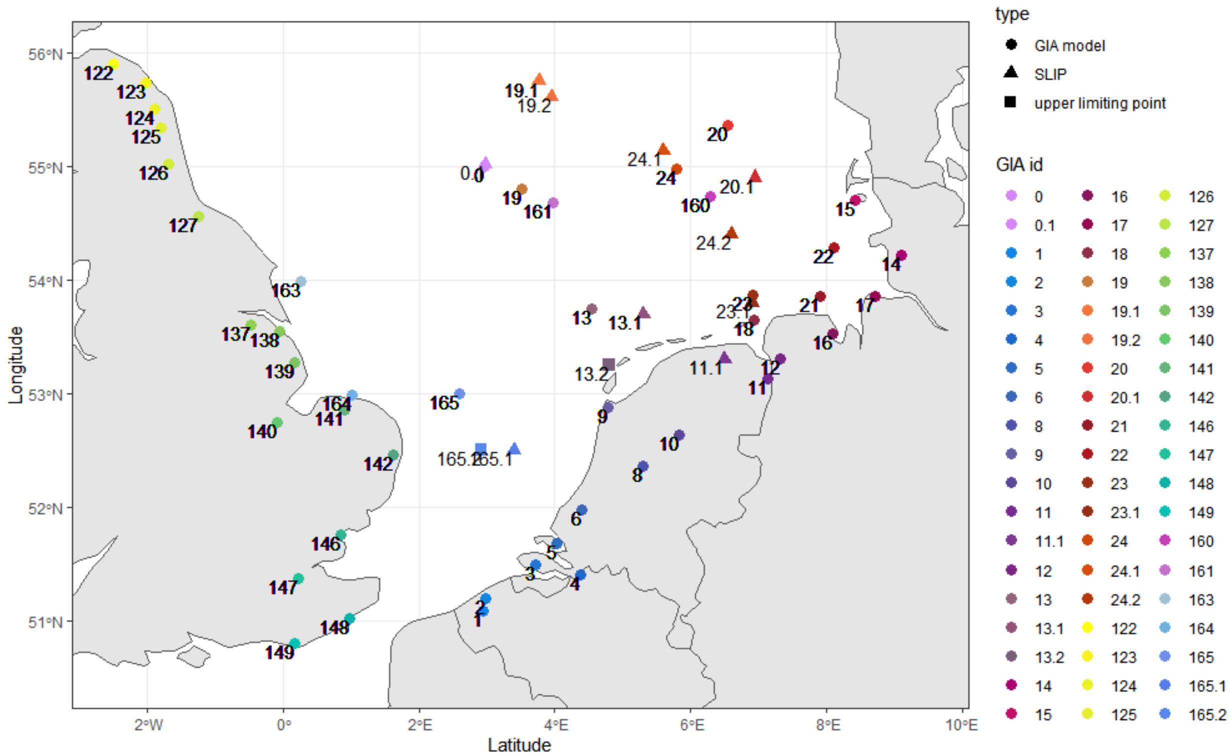

SI Figure 3.1: locations for GIA model curves from Kuchar (0) Shennan (122-165) and Vink (1-24). locations of SLIPs.

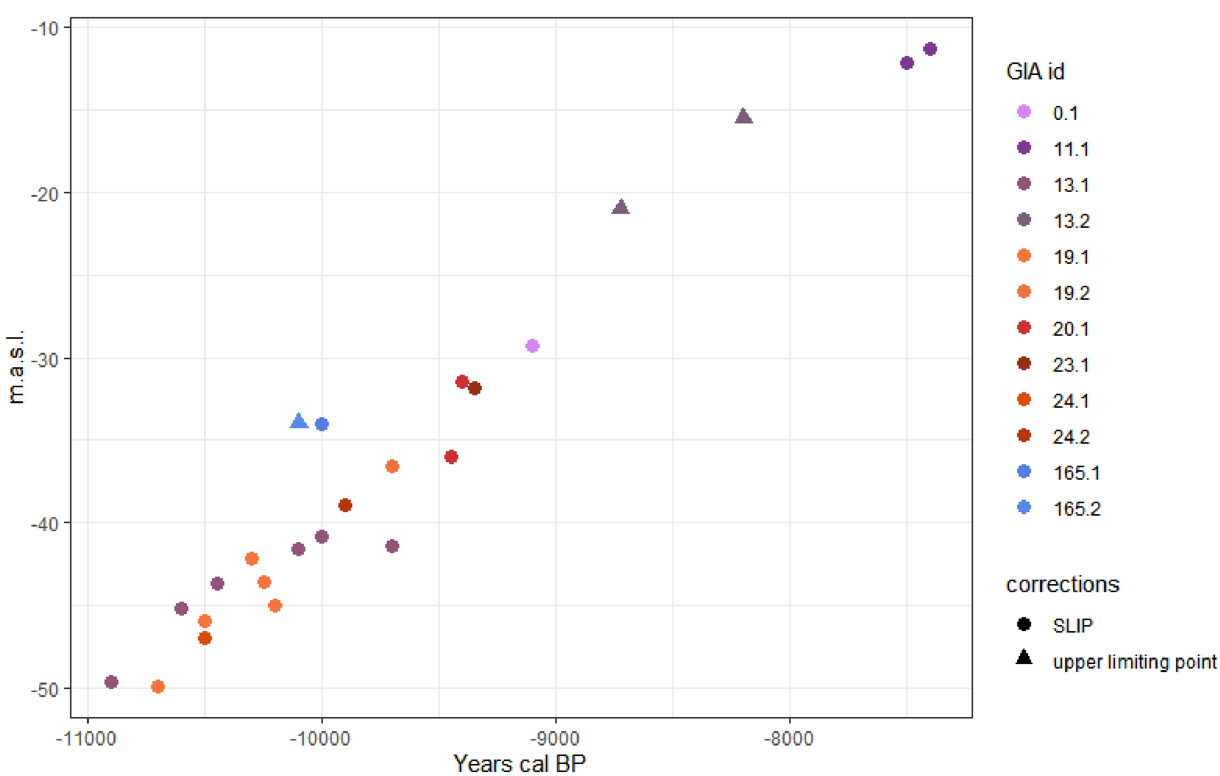

SI Figure 3.2: SLIPs used in the checking and nudging of central North Sea RSL curves.

3.2.1 Doggerbank

Figure 2a shows curves 0 and 19 are very close. Based on SLIP 0.1 (Hijma et al. 2012), and curve 19 (Vink et al. 2007), the latter part of the Kuchar et al. curve was corrected (10ka onwards) by adding half the difference between the depth values of 0 and 19 to curve 0. Several SLIPs were available to the Northeast (Fig. 1, 19.1, 19.2). For this location a new curve was made. The corrected curve 0 was used and fitted to the SLIPs for this location by subtracting the difference at 10.25 ka calBP (Fig. 2b). Shennan curves 160 and 161 are relatively deep and have been rejected as they don't fit well with the model output of Kuchar and Vink in this part of the north sea.

3.2.2 Oyster grounds

Several SLIPs and ULPs were available near the Frisian front / Oyster grounds (Vink et al. 2007 curve 13). SLIPS between 11 and 10ka calBP show a relatively good fit with curve 0. The difference between the SLIP at 10600 calBP and curve 0 was calculated and added, pushing this curve upwards. Then curve 13 was pushed downwards by subtracting the difference with curve 0 at 10k calBP and used from this timestep onwards (Fig. 3b)

3.2.3 Offshore Northeast Norfolk

The Shennan curve for offshore Northeast Norfolk (65) is relatively deep compared to SLIPs from the southern bight as well as the Oyster ground curve (13). The difference between the SLIP at 10ka and the curve was calculated and added to the depth at the timesteps up to that point. For the remaining timesteps 10k onwards, the added difference was diminished for each 50y timestep, leading up to a difference of 0 at 0 calBP.

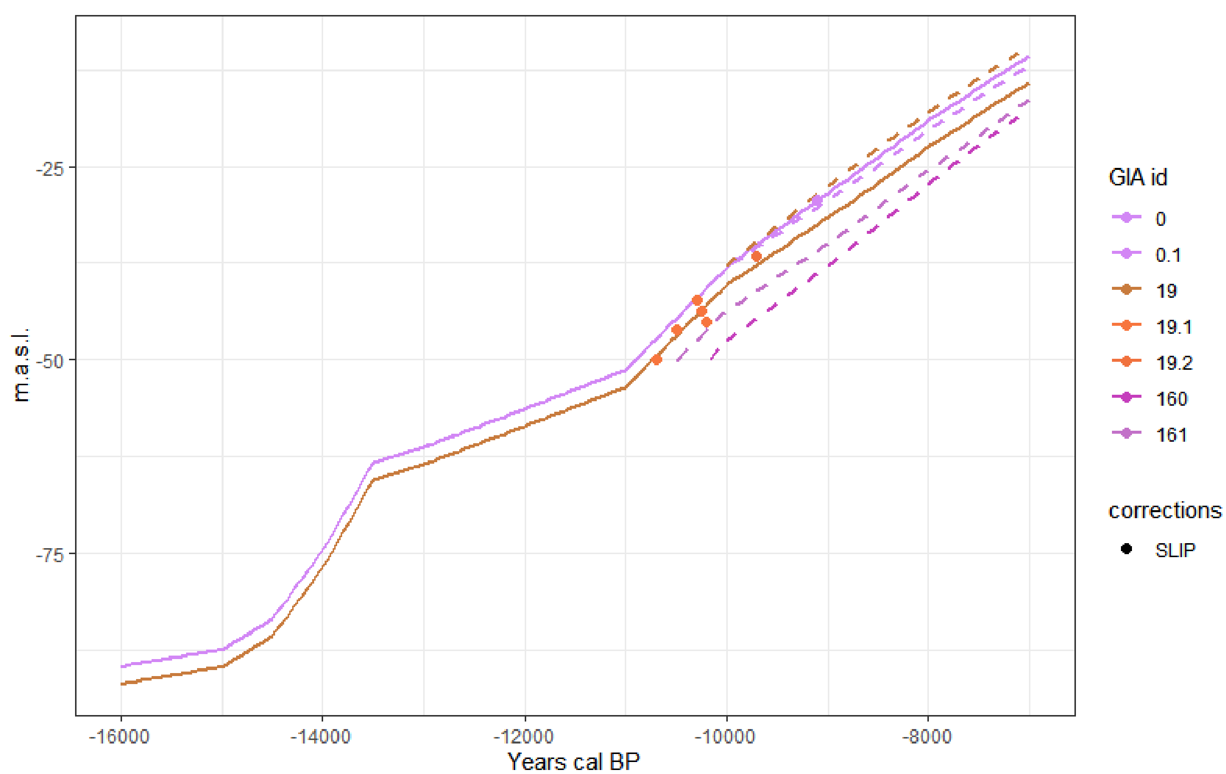

SI Figure 3.3 RSL curves for the Doggerbank: Kuchar 2012 (0), Vink (19), Shennan (61). Corrected RSL curves for the Doggerbank. Curve 160 and 161 were removed.

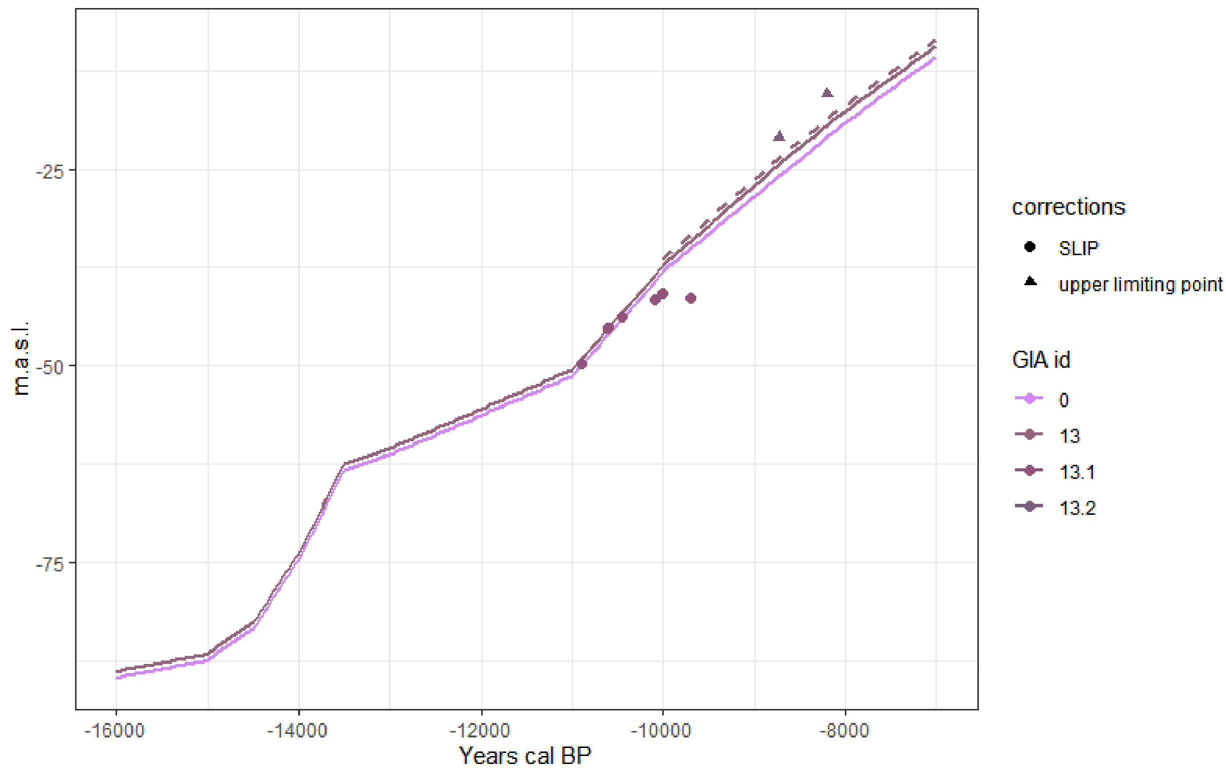

SI Figure 3.4: RSL curves for the Oyster Grounds (Vink et al. 2007 13) compared with the corrected Doggerbank curve (0) and SLIPs

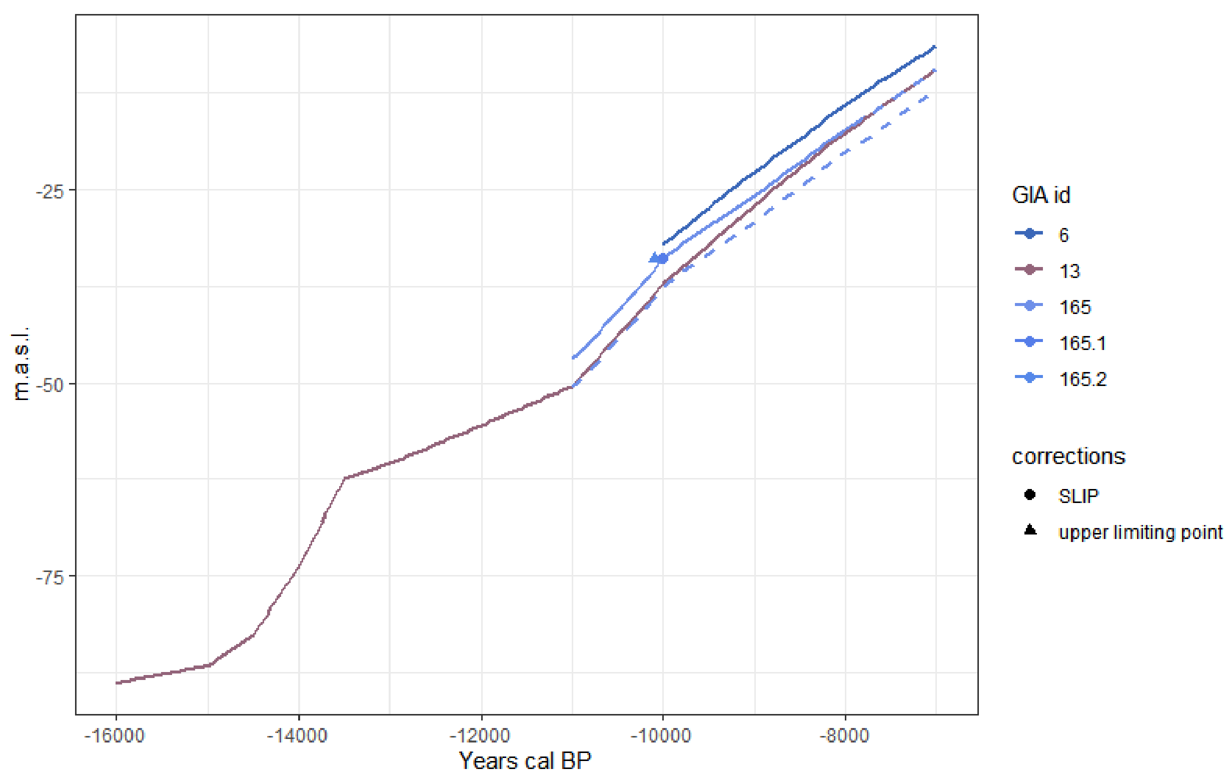

SI Figure 3.5: RSL curve for offshore NE Norfolk (Shennan 65). and SLIPs for the southern bight. b. corrected curve.

4 Radiocarbon

4.1 dataset description

The archaeological radiocarbon date dataset from Hoebe et al. 2023a was subjected to more stringent vetting (see Vermeersch 2023, Hoebe 2023b) and expanded with new data from Vermeersch 2022 (RPEv30), Van der Plicht & Kuitems 2022, and the p3k14c project (Bird et al. 2023). The final 3231 records in data24cal.xlsx contain information from an array of sources, listed in the source column for each record. Some sources contain unique data, but most dates are found across multiple sources. Table 4.1 shows the distribution of dates across the different sources in the dataset.

source group	Row Labels	Description	selected dates	data from multiple sources	dates unique to source
c14bazAAR	BDA	Base de Données Archéologiques by Thomas Perrin (1994).	21	17	4
c14bazAAR	CALPAL	Radiocarbon Database of the CalPal software package by Bernhard Weninger	1148	905	243
c14bazAAR	Euroevol	Cultural Evolution of Neolithic Europe Dataset by Manning et al. 2016	15	10	5
c14bazAAR	p3k14c	p3k14c: A synthetic global database of archaeological radiocarbon dates by Bird et al. 2023	136	132	4
c14bazAAR	PACEA	PACEA Geo-Referenced Radiocarbon Database for the late Middle Paleolithic, Upper Paleolithic, and initial Holocene in Europe by d'Errico et al. 2011	315	298	17
c14bazAAR	RPE	Radiocarbon Palaeolithic Europe Database (P. Vermeersch).	280	232	48
national	ADS (UK)	Archaeology Data Service UK	497	397	100
national	RICH (Belgium)	Royal Institute for Cultural Heritage Belgium KIK/IRPA (Koninklijk Instituut voor het Kunstpatrimonium / Institut Royal du Patrimoine Artistique)	385	108	277
laboratory	CIO (Groningen)	Centrum voor Isotopen Onderzoek Groningen	1222	717	505
laboratory	ORAU (Oxford)	Oxford Radiocarbon Accellerator Unit	116	108	8
research database	Niekus Peeters	Mesolithic hearth pits	768	472	296
literature	Cziesla 2015	Grenzen im Wald	152	128	24
literature	Gehlen 2020	Mesolithic hearth pits	123	65	58
literature	PlichtKuitems 2022	North sea finds	52	35	17
literature	miscelaneous		571	506	65
		total:	**5230**	**3624**	**1606**
				unique data across multiple sources:	**1625**
				total dates:	**3231**

SI Table 4.1: source overview

4.1.1 NA Filling

The primary data often contains issues like missing site location or contextual data as well as differences and errors in formatting. Many sources contain (sometimes mismatching) information about the same dates. Missing information from one source can be supplemented by that of another source. To do this, labcode formatting was first unified (Xx-1234). By subsequent labcode matching and NA filling we ensured all relevant available column data from the different sources was retained. Sitenames were then also unified. Sitenames as they were listed in the source are given in the column sitename_source. An example of NA filling is given here for the column "wgslat"

```
# Find the most common "lat" value for each "labcode"
most_common_lat <- my_data %>%
  filter(!is.na(wgslat)) %>%
  group_by(labcode, wgslat) %>%
  summarise(count = n()) %>%
  arrange(desc(count)) %>%
  slice(1) %>%
  ungroup()

# Create a lookup table for labcode and the most common lat
lookup_table <- most_common_lat %>%
  select(labcode, wgslat)

# Merge the lookup_table with the original dataset to fill NA values in "lat"
filled_data <- my_data %>%
  left_join(lookup_table, by = "labcode") %>%
  mutate(wgslat = ifelse(is.na(wgslat.x), wgslat.y, wgslat.x)) %>%
  select(-wgslat.x, -wgslat.y)

# check the difference
NA_lat <- my_data %>%
  filter(is.na(wgslat))
na_lat_fi <- filled_data %>%
  filter(is.na(wgslat))

my_data <- filled_data
```

4.1.2 Appending other data

In GIS, missing location data was appended manually for the remaining dates without coordinates. The sites were divided into a western and eastern selection. The dataset was then prepared by calibrating in rcarbon (Crema & Bevan 2020) using Intcal20 (Reimer et al. 2020). Calibrated date ranges are added as columns (calBP_start, calBP_end) as well as date range (dlength) and the corresponding chronozone. Dates were binned into site phases using an h value of 100 years and bins were added as a column. An overview of the number of dates for different categories is given in the script '1 Dataset overview.R', with the result shown in table 4.2.

selection	country	n.dates	n.phases	n.sites
west	Britain	617	437	226
east	Belgium	595	316	146
east	Netherlands	1479	815	346
east	Germany	540	290	129
full	**Total**	**3231**	**1858**	**847**

SI Table 4.2: distribution of dates, phases and sites across

4.2 Analysis

All analyses of the radiocarbon dataset was done on binned, non-normalised data in rcarbon (Crema & Bevan 2021). First, using kernel density estimation (sampleDates(), ckde()) across 500 simulations with a bandwidth of 50 years. This was done for the total, western and eastern datasets separately (‘2 Frequency distribution.R’). Then spatial analysis was done (‘3 Spatial analysis.R’) following Crema et al. (2017). First rate of change between the 250y timesteps was calculated for the whole dataset (spd2rc()) against which the local growth rates in the dataset could be compared. The spatial permutation test (sptest(), 100 simulations) involves first calculating distances between sites (spDists()) based on xy coordinates, then assigning weights to the sites based on the nearness of other sites in space and time (spweights(), using h=100 and a gaussian kernel). Example output is given in figure 4.1 at 9.25ka. Test results (SI-4.1 left) give p and q values for positive (orange, red) and negative (light blue, dark blue) local deviations from the overall growth rate during the timestep (figure SI-4.1 right), corresponding to the rate of change results (Figure 14 in main text). The full output is given in a separate SPT results pdf.

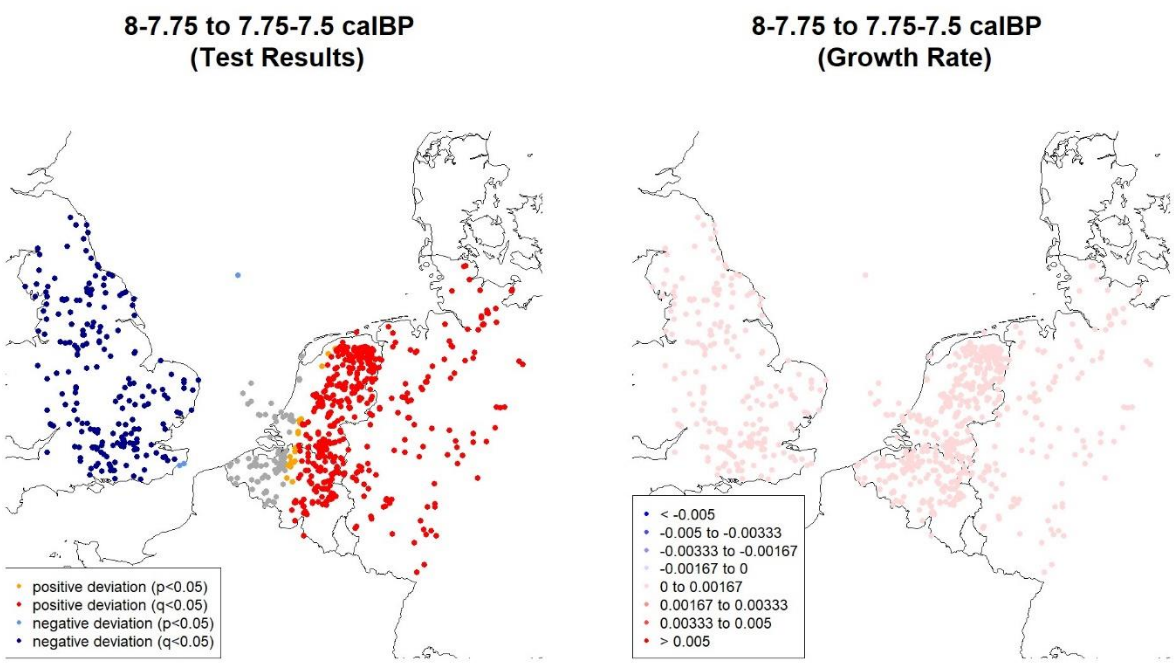

SI Figure 4.1: test results and growth rate between the 8-8.75ka timestep and the 8.75-7.5ka timestep.

Finally, mark permutation testing was performed (‘4 Mark permutation tests.R’) and compared to the inundation model histogram output (SI-1.4, ‘inundation rate.R’). The used categories in permutation testing were lowland and inland, with a boundary set at 50 meters above past sea level according to IM112 output. This modelled elevation data was extracted in QGIS from IM112 output with raster sampling (‘sitedata sample raster.py’). The elevation category for each 250y timestep was added to each radiocarbon date record. Then, for each record, only the elevation data for the timestep matching the date was retained. The lowland and inland marks were added to the data (“low” and “high”). Rate of change was calculated for the eastern dataset (spd2rc(), see figure SI-4.2). Mark permutation testing (permTest()) was then done across 500 simulations and with a running mean of 50 years. An overview of the number of sites per category is given in table 4.3.

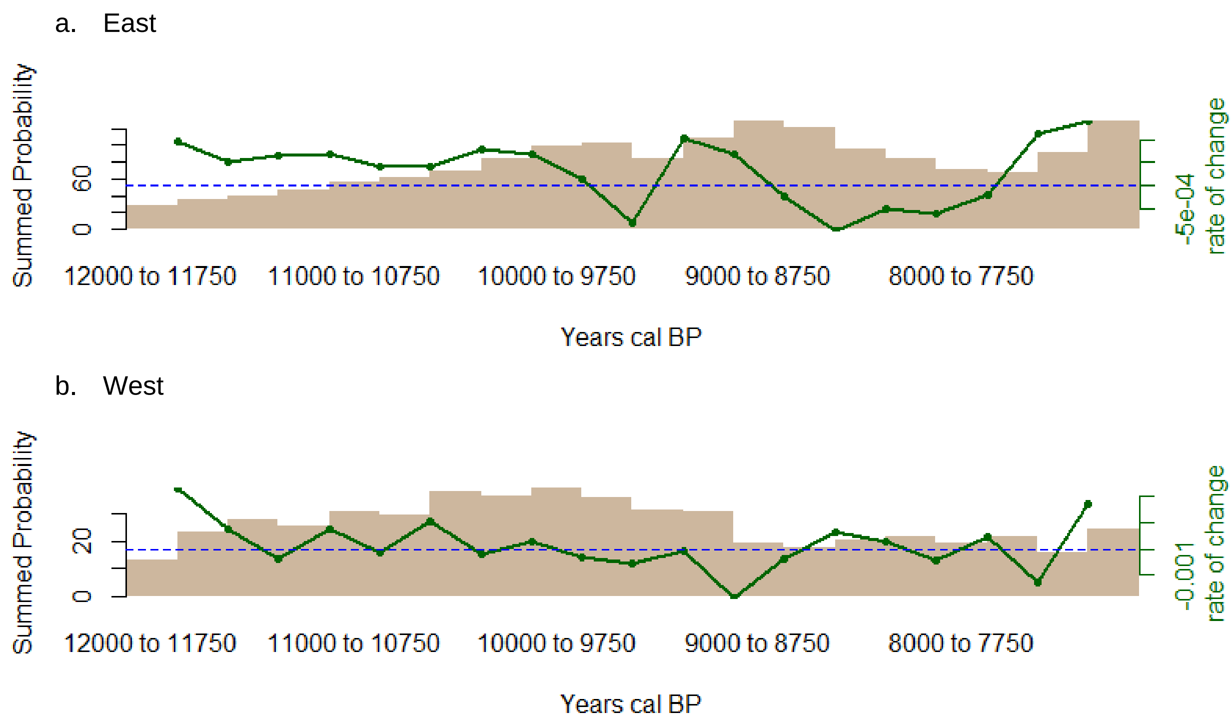

SI Figure 4.2: rate of change for the eastern and western dataset.

selection	landscape	dates	phases	sites
full		**3231**	**1858**	**847**
east		**2695**	**1416**	**621**
	lowland	1601	824	350
	inland	1094	667	361
west		**631**	**436**	**225**
	lowland	158	109	62
	inland	473	340	176

SI Table 4.3 number of sites per landscape category.

SI references

Bird, D., Miranda, L., Vander Linden, M., Robinson, E., Bocinsky, R. K., Nicholson, C., Capriles, J. M., Finley, J. B., Gayo, E. M., Gil, A., d'Alpoim Guedes, J., Hoggarth, J. A., Kay, A., Loftus, E., Lombardo, U., Mackie, M., Palmisano, A., Solheim, S., Kelly, R. L. & Freeman, J. (2022). p3k14c, a synthetic global database of archaeological radiocarbon dates. Sci Data 9: 27.

Bradley, S. L. (2011). Using sea-level and land motion data to develop an improved glacial isostatic adjustment model for the British Isles, Durham University.

Bradley, S. L., Milne, G. A., Shennan, I. & Edwards, R. (2011). An improved glacial isostatic adjustment model for the British Isles. J. Quaternary Sci. 26: 541–552.

Brooks AJ, Bradley SL, Edwards RJ, et al. 2008. Postglacial relative sealevel observations from Ireland and their role in glacial rebound modelling. Journal of Quaternary Science 23: 175–192.

Crema, E. R. & Bevan, A. (2021). Inference from large sets of radiocarbon dates: software and methods. Radiocarbon 63: 23–39.

Crema, E. R., Bevan, A. & Shennan, S. (2017). Spatio-temporal approaches to archaeological radiocarbon dates. Journal of Archaeological Science 87: 1–9.

De Clercq, M. (2018). Drowned Landscapes of the Belgian Continental Shelf. Implications for northwest European landscape evolution and preservation potential for submerged heritage, Ghent University.

De Clercq, M., Chademenos, V., Van Lancker, V. & Missiaen, T. (2016). A high-resolution DEM for the Top-Palaeogene surface of the Belgian Continental Shelf. Journal of Maps 12: 1047–1054.

Dziewonski, A.M., Anderson, D.L., 1981. Preliminary reference Earth model. Physics of the Earth and Planetary Interiors 25, 297–356.

Farrell WE, Clark JA. 1976. Postglacial sea-level. Geophysical Journal of the Royal Astronomical Society 46: 647–667.

Hijma, M. P., Cohen, K. M., Roebroeks, W., Westerhoff, W. E. & Busschers, F. S. (2012). Pleistocene Rhine-Thames landscapes: geological background for hominin occupation of the southern North Sea region. J. Quaternary Sci. 27: 17–39.

Hoebe, P. W., Peeters, J. H. M. & Arnolddusen, S. (2023). Reply to Vermeersch's comment on Hoebe et al. 2023. Parsing prehistoric patterns. Journal of Archaeological Science: Reports 52: 104229.

Kendall RA, Mitrovica JX, Milne GA. 2005. On post-glacial sea level. II. Numerical formulation and comparative results on spherically symmetric models. Geophysical Journal International 161: 679–706.

Kuchar, J., Milne, G., Hubbard, A., Patton, H., Bradley, S., Shennan, I. & Edwards, R. (2012). Evaluation of a numerical model of the British–Irish ice sheet using relative sea-level data: implications for the interpretation of trimline observations. J Quaternary Science 27: 597–605.

Mitrovica JX, Milne GA. 2003. On post-glacial sea level. I. General theory. Geophysical Journal International 154: 253–267.

Shennan, I., Bradley, S. L. & Edwards, R. (2018). Relative sea-level changes and crustal movements in Britain and Ireland since the Last Glacial Maximum. Quaternary Science Reviews 188: 143–159.

Steffen, H. & Kaufmann, G. (2005). Glacial isostatic adjustment of Scandinavia and northwestern Europe and the radial viscosity structure of the Earth's mantle. Geophysical Journal International 163: 801–812.

Van der Plicht, J. & Kuitems, M. (2022). Fossil bones from the North Sea: Radiocarbon and stable isotope (13C/15N) data. Radiocarbon 64: 633–668.

Vermeersch, P. M. (2023). Comment on P.W. Hoebe, J.H.M. Peeters, S. Arnoldussen. Parsing prehistoric patterns: Prospects and limitations of a big radiocarbon dataset for understanding the impact of climate on Late Palaeolithic and Mesolithic populations in northwest Europe (16–7.5 ka calBP). Journal of archaeological Science: Reports 49 (2023) 103,944. Journal of Archaeological Science: Reports 52: 104054.

Vink, A., Steffen, H., Reinhardt, L. & Kaufmann, G. (2007). Holocene relative sea-level change, isostatic subsidence and the radial viscosity structure of the mantle of northwest Europe (Belgium, the Netherlands, Germany, southern North Sea). Quaternary Science Reviews 26: 3249–3275.

Westerhoff, W.E., Wong, Th.E., De Mulder, E.F.J. 2003. Opbouw van de ondergrond. Deel 3. In: De Mulder, E.F.J., Geluk, M.C., Ritsema, I., Westerhoff, W.E., Wong, Th.E. (eds.): De ondergrond van Nederland. Netherlands Institute of Applied Geosciences TNO - National Geological Survey, 249-352.

5 Inundation model output

Inundation model output is given in a separate pdf (Inundation model output.pdf). Each output set gives the output of a bathymetry based model and a paleoDEM based model, with different sealevel and correction factors. See table below for reference.

	Inundation model		DEM		SL		Correction		
			0 BATHY	1 pDEM	0 ESL	1 SLL	0 NA	1 VLM	2 peat
page	2-3	IM000	x		x		x		
		IM100		x	x		x		
page	4-5	IM010	x			x	x		
		IM110		x		x	x		
page	6-7	IM011	x			x		x	
		IM111		x		x		x	
page	8-9	IM012	x			x		x	x
		IM112		x		x		x	x